Technical note: Facilitating the use of low-cost methane (CH$_4$) sensors in flux chambers – calibration, data processing, and an open source make-it-yourself logger

5 David Bastviken[1], Jonatan Nygren[1], Jonathan Schenk[1], Roser Parellada Massana[1], Nguyen Thanh Duc[1]

[1]Department of Thematic Studies – Environmental Change, Linköping University, 58183 Linköping, Sweden

Correspondence to: David Bastviken (david.bastviken@liu.se)

Abstract. A major bottleneck regarding the efforts to better quantify greenhouse gas fluxes, map sources and sinks, and
10 understand flux regulation, is the shortage of low-cost and accurate-enough measurement methods. The studies of methane
(CH$_4$) – a long-lived greenhouse gas increasing rapidly but irregularly in the atmosphere for unclear reasons, and with poorly
understood source-sink attribution – suffer from such method limitations. This study present new calibration and data
processing approaches for use of a low-cost CH$_4$ sensor in flux chambers. Results show that the change in relative CH$_4$ levels
can be determined at rather high accuracy in the 2 – 700 ppm mole fraction range, with modest efforts of collecting reference
15 samples *in situ*, and without continuous access to expensive reference instruments. This opens possibilities for more affordable
and time-effective measurements of CH$_4$ in flux chambers. To facilitate such measurements, we also provide a description for
building and using an Arduino logger for CH$_4$, carbon dioxide (CO$_2$), relative humidity, and temperature.

1 Introduction

Methane (CH$_4$) is the second most important of the long-lived greenhouse gases (GHGs). Its global warming potential per
20 mass on a 100-year time horizon (GWP$_{100}$) is 28-34 times greater than the GWP$_{100}$ for carbon dioxide (CO$_2$), and its relative
increase in the atmosphere since 1750 has been much greater than for other GHGs (e.g. Myhre et al., 2013). The atmospheric
CH$_4$ originates from multiple sources including incomplete combustion, handling natural gas or biogas, or microbial CH$_4$
production in agriculture, ruminant digestive tracts, and other anaerobic environments such as wetlands and lakes – the
microbial CH$_4$ accounting for approximately two thirds of the total emissions (Saunois et al., 2016). The high diversity of
25 sources, many yielding fluxes that have high spatio-temporal variability, makes it difficult to quantify fluxes and understand
flux regulation without a large number of local measurements. At the same time, common methods to measure fluxes rely on
expensive equipment or labour-demanding procedures. Consequently, the CH$_4$ flux from various sources is poorly constrained.
This is exemplified by the discovery of inland waters and flooded forests as two large global CH$_4$ sources during the last
decade (Bastviken et al., 2011;Pangala et al., 2017). Greater availability of measurement approaches that are inexpensive
30 enough to allow many measurements and assessment of both spatial and temporal variability simultaneously, would greatly
improve our ability to assess landscape CH$_4$ fluxes and flux regulation.

There is substantial interest in sensitive, small, and affordable CH_4 sensors, but so far the commercially available low-cost CH_4 sensors were typically developed for explosion warning systems and thereby for high concentrations (mole fractions at percent levels). CH_4 detection at percent levels is of high interest for environmental research, including the measurements of CH_4 ebullition, and for such applications cost-efficient sensor applications have been presented (e.g. Maher et al., 2019). For measurements of other types of CH_4 fluxes, sensors with robust and reliable detection at lower levels (mole fractions in the ppm range) are needed. Previous attempts to use and calibrate such sensors at ppm levels have been promising (Eugster and Kling, 2012), but also reported remaining challenges, and the use of these sensors in environmental research or monitoring has not yet become widespread. The direct monitoring of atmospheric CH_4 mole fractions to resolve fluxes, demanding fast and accurate detection of changes in the order of 10ppb, still represents a challenge for low-cost sensors. However, relevant mole fraction ranges for flux chamber studies (2 – ~1000 ppm depending on environment, chamber type, and deployment times) appear within reach.

One commercially available low-cost sensor type, showing promising performance in previous studies, is represented by the TGS 2600 tin dioxide (SnO_2) semiconductor sensor family made by Figaro. This type of sensors has been evaluated multiple times at CH_4 mole fractions near ambient background air (from 1.8 to 9 ppm; different ranges in different studies; (Eugster and Kling, 2012;Casey et al., 2019;Collier-Oxandale et al., 2018;van den Bossche et al., 2017). Given their low cost, they performed surprisingly well under non-sulphidic conditions (H_2S may interfere with the sensors), although it was challenging to generate calibration models with $R^2 > 0.8$, and the reported interferences from e.g. relative humidity (RH) and temperature (T) were large (van den Bossche et al., 2017). We here evaluate one member of this sensor family for a larger CH_4 range (2-719 ppm), selected to be appropriate for use in automated and manual flux chambers. We propose further development of the equations suggested by the manufacturer for data processing, and provide guidance on how to address the sensor response to humidity (H), RH and T in flux chamber applications. We also describe a simple CH_4/CO_2/RH/T logger based on the evaluated sensors, an Arduino microcontroller, and a corresponding logger shield.

2 Methods

2.1 The CH₄ sensor

The sensor used in this study is the Figaro NGM 2611-E13, which is a factory pre-calibrated module based on the Figaro TGS 2611-E00. The factory calibration is made at 5000 ppm, 20 °C and 65% RH. The CH_4 mole fraction in the factory calibration is not relevant for applications near atmospheric concentration, but the NGM 2611-E13 is compact and ready-to-use, facilitating its integration with data loggers and equipment for flux measurements (eg. automated flux chambers; (Duc et al., 2013;Thanh Duc et al., 2019). The detection range given by the manufacturer is 500-10000 ppm, but the sensor has been used successfully for measuring indoor ambient concentrations of methane (2-9 ppm) (van den Bossche et al., 2017). The potential

of another similar sensor, the Figaro TGS 2600, for atmospheric concentration monitoring has been investigated (Eugster and Kling, 2012;Collier-Oxandale et al., 2018, Eugster et al., 2020). The main difference of the TGS 2611-E00, compared to the TGS 2600, is the presence of a filter that reduce the interference of other combustible gases with the sensor, making it more selective towards CH_4 (Figaro_TGS_2611-E00, REV: 10/13). The TGS 2611-E00 is also more than 10 times cheaper than the sensor used in (Duc et al., 2013) and its detection range is wider, allowing for reliable measurements of concentration above 1000 ppm, which makes the sensor potentially useful in both low- and high-emitting environments.

2.2 Calibration setup

The sensor evaluation set-up was designed to resemble real measurement conditions in floating flux chambers in aquatic environments. The sensors were placed in the headspace of a plastic bucket positioned upside down on a water surface in a tank. We used a 7L plastic bucket in which we located 20 TGS 2611-E13 sensors connected to electronic circuitry and sensor signal logging system described in detail separately (Thanh Duc et al., 2019). The chamber headspace was continuously pumped from the chamber, through the measurement cell of an Ultraportable Greenhouse Gas Analyzer (UGGA; Los Gatos Research), and then back to the chamber. The UGGA served as a reference instrument for CH_4. The air T and RH inside the chamber were measured with ten K33-ELG CO_2 sensors (Senseair) which have an accuracy of $\pm$ 0.4°C and $\pm$ 3% RH (Bastviken et al., 2015). The large number of K33-ELG sensors was due to a separate test of wireless data transfer (outside the scope of this work) and one K33-ELG sensor would have been enough for this CH_4 sensor study. The entire installation was placed in a climate room to allow for varying T, and thereby also absolute humidity (H) in the chamber headspace. T and H co-vary under field conditions in measurements near moist surfaces, so although T and H were not controlled independently, their variability under this calibration setup was reflecting flux chamber headspace conditions under *in situ* field conditions.

The CH_4 concentration in the chamber was changed by direct injections of methane into the chamber by syringe via a tube. The CH_4 concentrations during the calibration experiments ranged from 2 ppm to 719 ppm. We performed multiple separate calibration experiments at different T and RH levels ranging from 10 to 42 °C and 18 – 70 %. At temperatures below 20 °C the RH was usually 50 - 70 %, while at temperatures > 20 °C, RH ranged from 18 to 60 %. The highest absolute water vapour mole fraction was 35 000 ppm H_2O. Values were recorded once per minute. T and RH values form the K33-ELG sensors were averaged among all sensors (because all sensors were in the same chamber and we could not link specific K33-ELG sensors to specific CH_4 sensors).

The response time to changing chamber headspace CH_4 levels differed between the sensors situated in the chamber (responding rapidly), and the UGGA (delayed response time due to the residence time of the measurement cell and tubing). The reference instrument measurement cell was large enough to be influenced by CH_4 from the chamber over a certain time period (the measurement cell residence time), and if the concentration change in the chamber was more rapid, the data from the reference instrument and sensors become incomparable and need to be omitted to not bias the calibration. Therefore data were filtered

to remove periods of rapid changes when the different response times caused data offsets. Some sensor data were lost during parts of the experiments due to power, connection failure, or data communication issues. Altogether on an average, after data filtration, 619 – 930 data points from each sensor and the UGGA, respectively, were used for the evaluation (in total 20 CH_4 sensors evaluated).

2.2 Data processing and interpretation

The TGS 2611 SnO_2 sensing area responds to interaction with target gas molecules by exhibiting decreasing resistance (Figaro_Tech_Info_TGS2611, 2012). The sensing area is connected in series with a reference resistor (resistance referred to as R_L). The total circuit voltage (V_C) is 5V across both the sensing area and the reference resistor. The voltage across the reference resistor (V_L) therefore varies in response to how the sensing area resistance (R_S) varies. V_L is measured and reported as output voltage. The sensor response R_S is calculated from the following equation (Figaro_Tech_Info_TGS2611, 2012;Figaro_TGS_2611-E00, REV: 10/13):

$$R_S = \left(\frac{V_C}{V_L} - 1\right) \times R_L \tag{1}$$

The active sensor surface characteristics can differ among individual sensors, which makes individual sensor calibration necessary. Interference by water vapour and T has been previously shown (Pavelko, 2012;van den Bossche et al., 2017). R_L is therefore ideally determined in dry air containing no volatile organic compounds or other reduced gases at a standard T. However, it can be challenging to achieve such conditions and determine R_L, and Eugster and Kling (Eugster and Kling, 2012) proposed to use the lowest measured sensor output voltage (V_0), representing minimum background atmospheric levels, to determine an empirical reference resistance R_0, and to calculate the ratio of R_S/R_0, reflecting the relative sensor response as follows:

$$\frac{R_S}{R_0} = \frac{\left(\frac{V_C}{V_L} - 1\right)}{\left(\frac{V_C}{V_0} - 1\right)} \tag{2}$$

This approach allows sensor use without accurate specific determination of R_L. Previous attempts to calibrate these type of sensors for environmentally relevant applications have focused on CH_4 mole fractions of 2-9 ppm, and typically considered the influence of T and RH or H (Casey et al., 2019;van den Bossche et al., 2017;Collier-Oxandale et al., 2018;Eugster and Kling, 2012). In these cases, an approximately linear response of the relative sensor response could be assumed due to the narrow CH_4 range. However, the sensor response is non-linear in the range relevant for flux chamber measurements and in this wider range, other approaches are needed. We here present a two-step sensor calibration based on the complete calibration

experiment data. In addition, we tried simplified calibration approaches for situations when full calibration experiments are not feasible and when access to reference instruments is limited. These approaches are described below.

2.2.1 Two-step calibration from complete experimental data (Approach I)

130 The first step (Step1) regards determination of the reference sensor resistance, R_0. We assumed that R_0 represented $R_L + R_{Sbkg}$, where R_{Sbkg} is R_S at the background atmospheric CH_4 level. We first tried the previously suggested approach to determine R_0 from the minimum V_L, i.e. setting V_0 to V_L at the lowest humidity and CH_4 concentrations during all measurements, thereby assuming that R_0 could be seen as constant. However, R_{Sbkg} may be influenced by H and T and could vary even if the CH_4 levels at background atmospheric conditions are constant. Thus, we also tested ways to correct R_0 to RH or H and T. Therefore,

135 after selecting the experiment data at background CH_4 levels but variable humidity and temperature, we tested linear, power, or Michaelis-Menten models, to generate V_0 values valid for different humidity and temperatures. This allowed estimation of R_0 values at the humidity and temperature associated with each R_S value, making the R_S/R_0 ratio less biased. The background level CH_4 data was selected in two different ways – either as all known CH_4 mole fractions below 2.5 ppm (n = 38-72), or as the minimum V_L value for each experiment and sensor (n = 6-7).

140

The second step (Step 2) regards calculation of CH_4 mole fractions from R_S/R_0. Several models were tested, where the CH_4 mole fraction were estimated as a function of R_S/R_0, H, T, and a constant to consider offsets that may differ among sensors. We tried several linear and power functions. In line with viewing the sensor surface as an active site where CH_4 and H_2O compete for space, the H effect was in some models represented as an interaction with the sensor response.

145 In all above cases, models were generated by curve-fitting in Python using the scipy.optimize curve_fit function. Predicted CH_4 mole fractions were evaluated by comparison with mole fractions independently measured by the UGGA. The specific model equations are provided in Table 1 and 2. We tested models using RH or H (which was calculated from RH and T; (Vaisala_Technical_Report, 2013). Each evaluation included a combination of both steps above, and generated one set of fitted parameters per sensor used, including the parameters for Step 1 and 2.

2.2.2 Simplified calibration approaches without dedicated calibration experiment data (Approach II and III)

150

The model combinations from Step 1 and 2 above that generated the best fit with the minimum number of parameters was selected for tests of two simplified calibration approaches. In *Approach II* we tested if model parameters in Step 2 can be predicted from parameters derived in Step 1, hypothesising that the derived model parameters in both Step 1 and Step 2 reflect the sensor capacity to respond to CH_4 and humidity levels as well as the individual sensor offset. If correct, the parameters in

155 Step 1 should be correlated with parameters in Step 2. If this correlation is strong enough, it may be possible to predict parameters in Step 2 from parameters in Step 1, which can be derived from measurements at background air concentrations under the natural variation in humidity (e.g. the diel variability), as a part of the regular measurements, preferentially using data when the atmospheric boundary layer is well mixed (e.g. windy conditions). Under such conditions atmospheric

background CH_4 concentrations can be relatively accurately assumed. Hence this Approach II would not require access to sensor calibration chambers, nor expensive reference gas analysers, which in turn would make sensor measurements available much more broadly. To test this approach, we searched for the best possible regression equations to predict Step 2 parameters from Step 1 parameters, then used these equations to estimate CH_4 mole fractions, and compared this with the UGGA reference measurements.

In *Approach III* we evaluated if reasonable accurate Step 1 and 2 equations can be derived from the combination of (*i*) minimum background atmospheric level V_L at different humidity, and (*ii*) a limited number of randomly collected independent manual flux chamber samples. If so, a few manual samples during the regular measurements could replace tedious dedicated calibration experiments. To test this approach the calibration data for each sensor was subsampled randomly and this random subset data were combined with the minimum V_L data to derive calibration parameters as done in Approach I. Using these parameters, the CH_4 mole fractions for the entire calibration data was estimated and compared with observed values. Monte Carlo simulations were run to test effects of the number of random reference samples (1 – 50) and the methane concentration ranges (3 – 500 ppm, or 3-50 ppm, respectively) in the subset data.

2.2.3 A low-cost Arduino-based CH_4/CO_2/*RH*/*T* logger

To facilitate use of the sensors and our results, we also gathered instructions for how to build a logger for CH_4, CO_2, *RH* and *T* measurements, using the CH_4 sensor tested here, and the Senseair K33 ELG CO_2/*RH*/*T* sensor described elsewhere (Bastviken et al., 2015), a supplementary DHT22 sensor for *RH* and *T*, an Arduino controller unit, and an Adafruit Arduino compatible logger shield with a real time clock (input voltage 7-12 V; 10 bit resolution; Figure 2). This development was based on sensor specifications and the open source knowledge generously shared on internet by the Arduino user community. The full description of this logger unit is found in the Supplement.

3 Results and Discussion

The results of different Step 1 and Step 2 calibration equations are shown in Tables 1 and 2. The models including *H* were equal or superior to models using *RH*. This is reasonable because it is the absolute water molecule abundance that influence the sensor response. Hence, models using *H* were prioritized. In Approach I, several Step 1 models, including a constant minimum V_L, and power, linear and Michaelis-Menten-based equations gave similar R^2 (0.85 to 0.9) and root mean square error (RMSE) when comparing predicted versus observed results (Table 1). The effect of *T* appeared negligible compared to *H*, which may be related to the built-in heating of the active sensor surface (280 mW; this heating was focused on a small part of the sensor and no self-heating around sensors was detected). It is possible that the Michaelis-Menten equation is superior over the full theoretically possible *H* range. However, under our experiment conditions, covering normal field *H* levels, the

combination of best fit and minimum number of parameters in Step 1, was found for a simple linear equation with *H* (Model V4 in Table 1), which was used for later tests of Approach II and III.

The tests of different equations in Approach I, Step 2, showed that power relationships with *H* and *T* represented as interactions with the sensor response, performed best (Table 2 Model ≥4). With the exception of Models 10a-c, all these models had in the regression of observed versus predicted, a slope and intercept that was statistically indistinguishable from 1 and 0, respectively ($p < 0.05$) and an R^2 of 0.98 – 1.00 (Table 2, Figures S1 and S2). Again, *T* had a marginal effect and *H* was clearly most important. Hence, while Model 7 including *T* in Table 2 had the lowest RMSE (9.8), Model 8 represented a good compromise between minimum number of parameters and low RMSE (10.4) and was used in Approach II and III. The non-linear response of the sensor yielded a stronger and more coherent response at low CH_4 levels, and a large part of the uncertainty were generated at the higher CH_4 levels in the studied range (Figures S1 and S2). Near the atmospheric background at 2 ppm, the confidence interval for individual sensor response was in the order of ± 1.1 ppm (Model 7 having lowest RMSE). Hence, the presented calibration equations have a limited accuracy in terms of absolute CH_4 mole fractions, and is not optimized for high-precision measurements at atmospheric background levels (as shown by SE for the model intercept corresponding to 0.16-1 ppm; Table 2). However, high R^2 and low SE for the slope of several models indicate that the relative change of CH_4 levels over time, which is the core of flux chamber measurements, can be assessed efficiently with the sensors if calibrated properly (Table 2).

Approach II, deriving all calibration equations from a small set of minimum V_L values using Models V4 or V5 (Table 1) and 10a-c (Table 2), generated substantially greater RMSE. Most of this RMSE change was due to less accurate prediction of the intercept. The R^2 and slope standard error range remained similar to the other models (Table 2), but the actual slope values could deviate substantially from 1 and varied considerably among sensors (in contrast to the models for all other approaches always having slopes close to 1 and similar among sensors; Figures S1 and S2). Thereby, Approach II could lead to a large bias in absolute mole fractions, and this crude generation of calibration equations may be adequate primarily for assessing relative change over time measured by the same sensor, and cross comparisons among sensors should be avoided when using this approach. Examples of equations for the parameter estimation in Approach II are provided in Table S1. Applying Approach II on a smaller concentration range yielded a considerably lower RMSE (Table 2, Model 10c).

Approach III (Model 11a and 11b in Table 2) showed that as few as 10 – 20 reference samples, collected at random occasions during actual measurements, could substantially reduce the RMSE of the calibration models, reaching close to the lowest levels based on the 619 – 930 measurements and the full range up to 719 ppm in Approach I (Table 2 Model 11a; Figure S3). The concentrations of the reference samples did not appear important for the RMSE within a given specific data range. However, simulations using data for CH_4 mole fractions below 50 ppm only, generated much lower RMSE than using all data (Table 2,

Model 11b). This support the conclusion that the sensors are more sensitive and give a stronger relative response in the low part of the studied concentration range.

225 An overview of approaches to derive calibration models for this type is shown in Table S1. The challenges found regarding monitoring of background atmospheric levels was confirmed by our study, while use for relative changes of greater magnitudes in flux chambers appear promising based on our results, also with a simplified calibration (Approach III). As a general note for all approaches when used under variable environmental conditions, best precision may be achieved by using absolute partial pressure units for both CH_4 and humidity, thereby compensating for variability in atmospheric pressure. In addition, for

230 use above the maximum absolute humidity in this study, extra care is advised to check sensor capacity and behaviour. An example of real field data is provided in Figure 3. This example illustrate that the direct sensor response is heavily influenced by humidity and that the calibration equations shown in Table 1 and 2 are needed to reveal the CH_4 part of the sensor signal. Further, Figure 3 illustrates that sensors can be highly useful in very variable environments with rapid changes in humidity and when using data loggers with 10 bit resolution only. Optimal calibration procedures in stable environments and with higher

235 logger resolution would likely indicate better sensor performance, while we deliberately focused on calibration procedures closely linked to field use with inexpensive equipment to provide information of relevance for as many conditions as possible.

Long-term stability of the sensors were not addressed here but is important for environmental use. Other studies of the same type of sensors show promising results. For example, van den Bossche et al. (2017) found no drift over 31 days. Eugster et al.

240 (2020) using the similar Figaro TGS 2600 sensor for outdoor measurements over 7 years, concluded that the drift was in the order of 4–6 ppb/yr. This suggest that the sensor drift is modest even when exposed to variable weather over long time. However, it is possible that the drift can be faster under some conditions and regular drift checks are therefore advised.

4 Conclusions

The main conclusions can be summarized by the following:

245 • The tested CH_4 sensors are suitable for use in flux chamber applications if there are simultaneous measurements of relative humidity and temperature.

• Sensor-specific calibration is required.

• Occasional independent reference samples during regular measurements, can be an alternative to designated calibration experiments. Background atmospheric levels in combination in the order of $10 - 20$ *in situ* reference samples at other CH_4

250 levels, can yield rather accurate calibration models.

• For highest accuracy regarding absolute CH_4 concentrations, careful designated calibration experiments covering relevant environmental conditions are needed.

- These results, together with the increased accessibility of low-cost sensors and data logger systems (one example described in the Supplement), open supplementary paths toward improved capacity for greenhouse gas measurements in both nature and society.

5 Code and data availability

Python code for data evaluation and the calibration experiment data are available from the main author upon request. Please note that both the code and the data are specific for the experimental setup. The Python code needs modifications for use with other data, and the CH_4 sensor data cannot represent results from other sensors as sensor specific calibration is needed. The Arduino code for the $CH_4/CO_2/RH/T$ logger described in the supplement is available at http://urn.kb.se/resolve?urn=urn:nbn:se:liu:diva-162780.

6 Author contribution

DB and NTD designed and supervised the study. NTD designed and built the experimental setup, the sensor units and the data logging system. JN and NTD performed the calibration experiment. The analysis of the sensor data was led by DB with contributions from NTD, JS, and JN. DB and NTD developed the logger units presented in the supplementary material. RP helped to build and test logger units and drafted a user manual. DB wrote the first complete draft of the manuscript and led the manuscript development, with contributions from NTD, JS, RP, and JN.

7 Competing interests

There are no competing interests.

8 Acknowledgements

This work was funded by the European Research Council (ERC) under the European Union's Horizon 2020 research and innovation programme (grant agreement No 725546), and the Swedish Research Councils VR and FORMAS (grant no. 2016-04829 and 2018-01794, respectively). We thank Sivakiruthika Balathandayuthabani, Magnus Gålfalk, Balathandayuthabani Panneer Selvam, Gustav Pajala, David Rudberg, Henrique Oliveira Sawakuchi, Anna Sieczko, Jimmy Sjögren, and Ingrid Sundgren, for stimulating discussions regarding sensor use.

References

Bastviken, D., Tranvik, L. J., Downing, J. A., Crill, P. M., and Enrich-Prast, A.: Freshwater methane emissions offset the continental carbon sink, Science, 331, doi.org/10.1126/science.1196808, 2011.

280 Bastviken, D., Sundgren, I., Natchimuthu, S., Reyier, H., and Gålfalk, M.: Technical Note: Cost-efficient approaches to measure carbon dioxide (CO_2) fluxes and concentrations in terrestrial and aquatic environments using mini loggers, Biogeosciences, 12, 3849–3859, doi.org/10.5194/bg-12-3849-2015, 2015.

Casey, J. G., Collier-Oxandale, A., and Hannigan, M.: Performance of artificial neural networks and linear models to quantify
285 4 trace gas species in an oil and gas production region with low-cost sensors, Sensors and Actuators B: Chemical, 283, 504-514, doi.org/10.1016/j.snb.2018.12.049, 2019.

Collier-Oxandale, A., Casey, J. G., Piedrahita, R., Ortega, J., Halliday, H., Johnston, J., and Hannigan, M. P.: Assessing a low-cost methane sensor quantification system for use in complex rural and urban environments, Atmos. Meas. Tech., 11, 3569-
290 3594, doi.org/10.5194/amt-11-3569-2018, 2018.

Duc, N. T., Silverstein, S., Lundmark, L., Reyier, H., Crill, P., and Bastviken, D.: An automated flux chamber for investigating gas flux at water – air interfaces, Environ. Sci. Technol., 47 968–975, doi.org/10.1021/es303848x, 2013.

295 Eugster, W., and Kling, G. W.: Performance of a low-cost methane sensor for ambient concentration measurements in preliminary studies, Atmospheric Measurement Techniques, 5, 1925-1934, doi.org/10.5194/amt-5-1925-2012, 2012.

Eugster, W., Laundre, J., Eugster, J., and Kling, G. W.: Long-term reliability of the Figaro TGS 2600 solid-state methane sensor under low Arctic conditions at Toolik lake, Alaska, Atmospheric Measurement Techniques. 13, 2681-95.,
300 https://doi.org/10.5194/amt-2019-402, 2020.

Figaro_Tech_Info_TGS2611: Technical information for TGS2611, http://www.figarosensor.com/products/2611Dtl.pdf, 2012.

Product information TGS 2611-E00, REV: 10/13, www.figarosensor.com/product/docs/TGS%202611C00(1013).pdf, 2013
305
Maher, D. T., Drexl, M., Tait, D. R., Johnston, S. G., and Jeffrey, L. C.: iAMES: An inexpensive, Automated Methane Ebullition Sensor, Environmental Science & Technology, 53, 6420-6426, doi.org/10.1021/acs.est.9b01881, 2019.

Myhre, G., Shindell, D., Bréon, F.-M., Collins, W., Fuglestvedt, J., Huang, J., Koch, D., Lamarque, J.-F., Lee, D., Mendoza,
310   B., Nakajima, T., Robock, A., Stephens, G., Takemura, T., and Zhang, H.: Anthropogenic and Natural Radiative Forcing, in:
Climate Change 2013: The Physical Science Basis. Contribution of Working Group I to the Fifth Assessment Report of the
Intergovernmental Panel on Climate Change, edited by: Stocker, T., Qin, D., Plattner, G.-K., Tignor, M., Allen, S., Boschung,
J., Nauels, A., Xia, Y., Bex, V., and Midgley, P., Cambridge University Press, Cambridge, United Kingdom and New York,
NY, USA, 2013.

315

Pangala, S. R., Enrich-Prast, A., Basso, L. S., Peixoto, R. B., Bastviken, D., Hornibrook, E. R. C., Gatti, L. V., Marotta, H.,
Calazans, L. S. B., Sakuragui, C. M., Bastos, W. R., Malm, O., Gloor, E., Miller, J. B., and Gauci, V.: Large emissions from
floodplain   trees   close   the   Amazon   methane   budget,   Nature,   552,   230,   doi.org/10.1038/nature24639
https://www.nature.com/articles/nature24639#supplementary-information, 2017.

320

Pavelko, R.: The influence of water vapor on the gas-sensing phenomenon of tin dioxide–based gas sensors, in: Chemical
Sensors: Simulation and Modeling Volume 2: Conductometric-Type Sensors, edited by: Korotcenkov, G., Momentum Press,
New York, 297-330, 2012.

325   Saunois, M., Bousquet, P., Poulter, B., Peregon, A., Ciais, P., Canadell, J. G., Dlugokencky, E. J., Etiope, G., Bastviken, D.,
Houweling, S., Janssens-Maenhout, G., Tubiello, F. N., Castaldi, S., Jackson, R. B., Alexe, M., Arora, V. K., Beerling, D. J.,
Bergamaschi, P., Blake, D. R., Brailsford, G., Brovkin, V., Bruhwiler, L., Crevoisier, C., Crill, P., Covey, K., Curry, C.,
Frankenberg, C., Gedney, N., Höglund-Isaksson, L., Ishizawa, M., Ito, A., Joos, F., Kim, H. S., Kleinen, T., Krummel, P.,
Lamarque, J. F., Langenfelds, R., Locatelli, R., Machida, T., Maksyutov, S., McDonald, K. C., Marshall, J., Melton, J. R.,
330   Morino, I., Naik, V., O'Doherty, S., Parmentier, F. J. W., Patra, P. K., Peng, C., Peng, S., Peters, G. P., Pison, I., Prigent, C.,
Prinn, R., Ramonet, M., Riley, W. J., Saito, M., Santini, M., Schroeder, R., Simpson, I. J., Spahni, R., Steele, P., Takizawa,
A., Thornton, B. F., Tian, H., Tohjima, Y., Viovy, N., Voulgarakis, A., van Weele, M., van der Werf, G. R., Weiss, R.,
Wiedinmyer, C., Wilton, D. J., Wiltshire, A., Worthy, D., Wunch, D., Xu, X., Yoshida, Y., Zhang, B., Zhang, Z., and Zhu, Q.:
The global methane budget 2000–2012, Earth Syst. Sci. Data, 8, 697-751, 10.5194/essd-8-697-2016, 2016.

335

Thanh Duc, N., Silverstein, S., Wik, M., Crill, P., Bastviken, D., and Varner, R. K.: Greenhouse gas flux studies: An automated
online system for gas emission measurements in aquatic environments, Hydrol. Earth Syst. Sci. Discuss., 2019, 1-18,
10.5194/hess-2019-83, 2019.

340   Vaisala_Technical_Report: Humidity   conversion   Formulas.   Calculation   fromulas   for   humidity.,   Finland,   17,
https://www.hatchability.com/Vaisala.pdf, 2013.

van den Bossche, M., Rose, N. T., and De Wekker, S. F. J.: Potential of a low-cost gas sensor for atmospheric methane

345   monitoring, Sensors and Actuators B: Chemical, 238, 501-509, https://doi.org/10.1016/j.snb.2016.07.092, 2017.

Table 1: Model results for Step 1 of sensor calibration - i.e. the correction of reference output voltage (V_0 in the unit mV) in background air to humidity and temperature. V_{0min}, H, and T, represent the minimum V_0 for each sensor (mV), absolute humidity (ppm), and temperature (°C) during measurements in open air. The model parameters g, h, S, m and n are constants for each sensor derived by curve fitting. The model R^2 is the adjusted coefficient of determination (mean, minimum and maximum for the 20 sensors tested), and RMSE is then root mean square error. Equivalent models using relative humidity (RH; %) instead of H, returned lower R^2 and higher RMSE and are not shown. These Step 1 models were combined with the Step 2 models as noted in Table 2. N denotes number of values used. See text for details.

Model for V_0		Data	N	Observed vs. Predicted			
No.	Equation			R^2			RMSE
				mean	min	max	mean
V1	V_{0min} (constant)	Minimum V_0	1	-	-	-	-
V2	$V_0 = gH^h + mT^n + S$	All < 2.5 ppm CH$_4$	38 - 72	0.85	0.66	0.94	8.9
V3	$V_0 = gH + mT + S$	All < 2.5 ppm CH$_4$	38 - 72	0.88	0.68	0.95	8.2
V4a	$V_0 = gH + S$	All < 2.5 ppm CH$_4$	38 - 72	0.88	0.68	0.95	8.2
V4b	$V_0 = gH + S$	Min V_0 for each exp.	6 - 7	0.90	0.72	0.96	8.3
V5a	$V_0 = gH/(S + H)$	All < 2.5 ppm CH$_4$	38 - 72	0.88	0.70	0.96	8.0
V5b	$V_0 = gH/(S + H)$	Min V_0 for each exp.	6 - 7	0.89	0.71	0.96	8.3

360 **Table 2:** Model results for Step 2 of the data evaluation, i.e. the determination of methane (CH_4) mole fractions (ppm) from the sensor response expressed as R (corresponding to R_S/R_0) using different calibration models. (RH), H, and T as defined in Table 1. The model parameters a, b, c, d, e, f and K are constants for each sensor derived by curve fitting. The models were evaluated via a linear regression of *Observed* versus *Predicted* CH_4 mole fractions, where k and M are the slope and the intercept, respectively. SE denote standard error, R^2 the adjusted coefficient of determination (mean and minimum to maximum for the 20 sensors tested), and RMSE is the root mean square error

365 (ppm). The table show the most successful subset of all models tested. N = 619 – 930 per sensor in total and 203-313 for the data subset with CH4 mole fractions < 50 ppm. See text for details.

Model		V_0	CH_4	$Observed = k * Predicted + M$				
No.	Equation	mod	max	k	M		R^2	RMSE
			ppm	SE (min-max)	min to max*	SE (min-max)	mean (min-max)	mean (min-max)
1	$CH_4 = aR + b(RH) + cT + K$	V1	719	0.024-0.036	$-3.2 \cdot 10^{-7}$ to $3.5 \cdot 10^{-7}$	5.8-8.2	0.58 (0.54-0.68)	117 (104-127)
2	$CH_4 = aR^b + c(RH)^d + eT^f + K$	V1	719	0.006-0.010	$-8.8 \cdot 10^{-7}$ to $4.2 \cdot 10^{-7}$	1.6-2.6	0.96 (0.94-0.97)	35.9 (32-45)
3	$CH_4 = aR^b + c(RH)(aR^b) + dT(aR^b) + K$	V1	719	0.003-0.006	$-6.8 \cdot 10^{-7}$ to $9.3 \cdot 10^{-7}$	0.72-1.44	0.99 (0.98-0.99)	18.5 (15-25)
4	$CH_4 = aR^b + cH(aR^b) + dT(aR^b) + K$	V1	719	0.002-0.003	$-4.3 \cdot 10^{-7}$ to $3.2 \cdot 10^{-7}$	0.43-0.90	1.00 (0.99-1.00)	11.4 (9-16)
5	As No. 4	V2	719	0.001-0.003	$-3.3 \cdot 10^{-7}$ to $4.1 \cdot 10^{-7}$	0.38-0.87	1.00 (0.99-1.00)	10.6 (8-16)
6	As No. 4	V3	719	0.001-0.003	$-4.1 \cdot 10^{-7}$ to $3.6 \cdot 10^{-7}$	0.37-0.82	1.00 (0.99-1.00)	9.8 (8-15)
7	As No. 4	V4a	719	0.001-0.003	$-2.2 \cdot 10^{-7}$ to $2.8 \cdot 10^{-7}$	0.37-0.82	0.99 (0.99-1.00)	9.8 (8-14)
8	$CH_4 = aR^b + cH(aR^b) + K$	V4a	719	0.001-0.003	$-5.6 \cdot 10^{-7}$ to $1.3 \cdot 10^{-7}$	0.37-0.84	1.00 (0.99-1.00)	10.4 (8-15)
9a	As No. 8 with equation V4b to determine V0.	V4b	719	0.001-0.003	$-7.8 \cdot 10^{-7}$ to $1.4 \cdot 10^{-6}$	0.37-0.84	1.00 (0.99-1.00)	10.4 (8-15)
9b	As No. 9a with lower max CH4 level.	V4b	50	0.007-0.014	$-4.1 \cdot 10^{-8}$ to $8.1 \cdot 10^{-8}$	0.16-0.33	0.98 (0.96-0.99)	2.1 (2-3)

10a	As No 8. Parameters a, b, c and K estimated from relationships with parameters in V4b; see text.	V4b	719	0.001-0.012	-108 to 1.1	0.39-1.62	1.00 (0.99-1.00)	74 (18-150)
10b	As No 8. Parameters a, b, c and K estimated from relationships with parameters in V5b; see text.	V5b	719	0.001-0.024	-122 to 1.9	0.43-2.80	0.99 (0.96-1.00)	88 (20-154)
10c	As No. 10a with lower max CH_4 level.	V4b	50	0.006-0.021	-51 to -14	0.30-0.87	0.98 (0.96-0.98	28 (21-35)
11a	As No. 8. Parameters a, b, c, and K, *derived* from 6-7 minimum V_L values at different H, and 20 samples at random CH_4 mole fractions between 3 and 500 ppm.**	V4b	719	0.002-0.004	-6.5 to 7.1	0.41-0.96	1.00 (0.99-1.00)	13 (8.8-20)
11b	As No. 11a with the 20 random samples at CH_4 mole fractions between 3 and 50 ppm.**	V4b	50	0.008-0.017	-0.7 to 0.5	0.17-0.41	0.97 (0.95-0.98)	2.5 (2-3)

*Minimum and maximum mean intercepts for the group of 20 sensors. The confidence interval around the mean intercept was ± 1.1 ppm in Model 7 (having lowest RMSE). ** Monte Carlo simulations with 1000 runs generating random data subsets used for deriving the model parameter ranges.

370
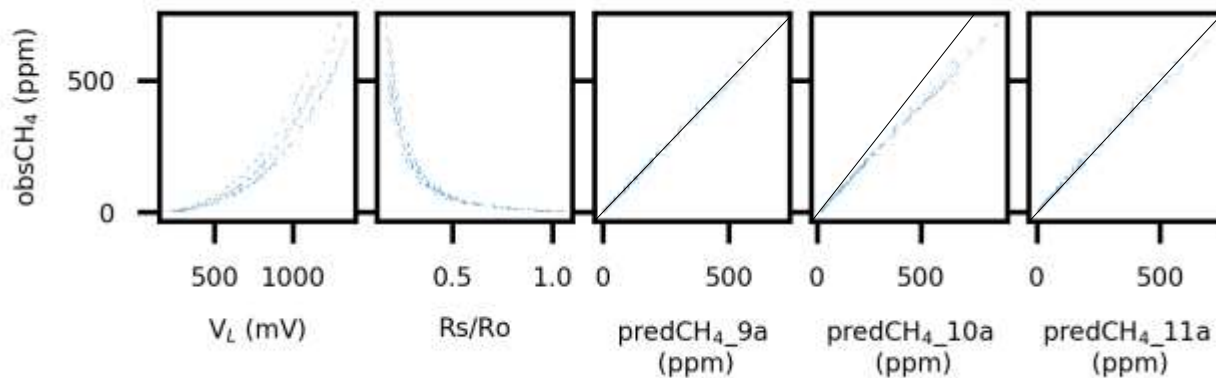
375

Figure 1. Sensor output voltage (V_L; mV), Rs/R_0 ratio, and predicted CH$_4$ mixing ratio (predCH$_4$; ppm) using Model 9a, 10a and 11a in Table 2, respectively, versus observed CH$_4$ mixing ratio (obsCH$_4$; ppm), for one of the studied sensors. See text for details and Figures S1 and S2 for similar graphs regarding all sensors. Black diagonals represent 1:1 lines.

380
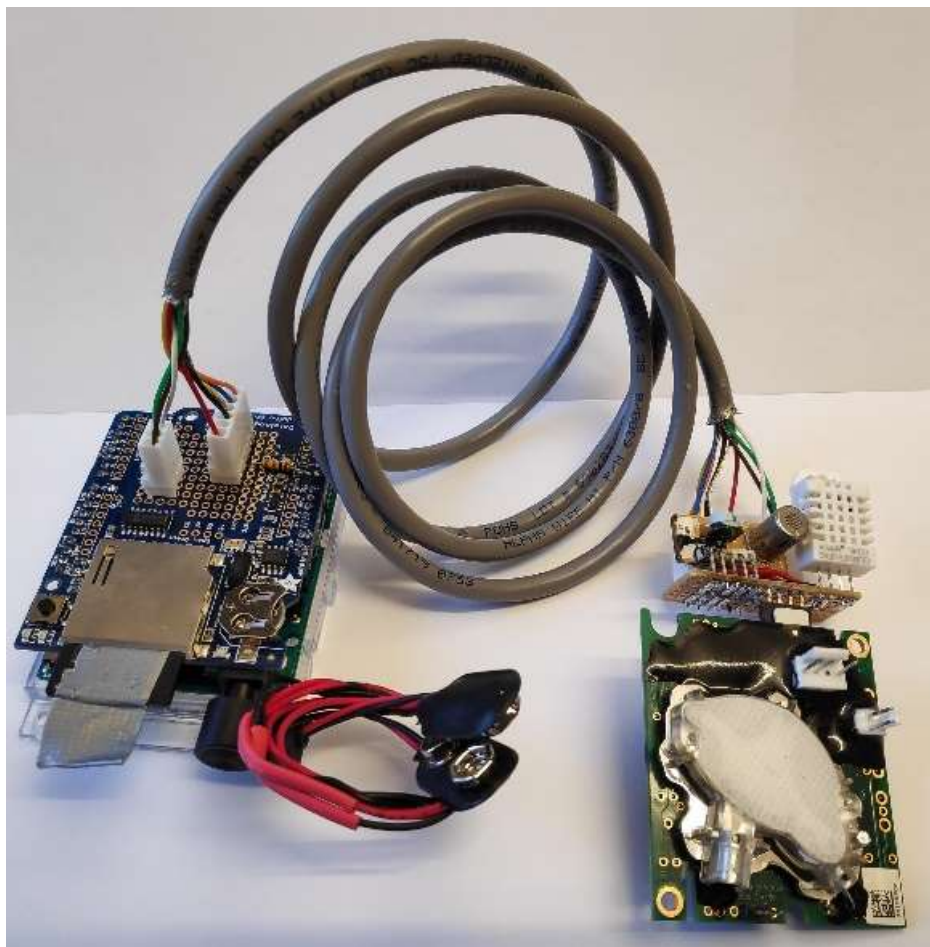
385

Figure 2. Photo of the CH$_4$/CO$_2$/RH/T logger described in the supplementary information.

390
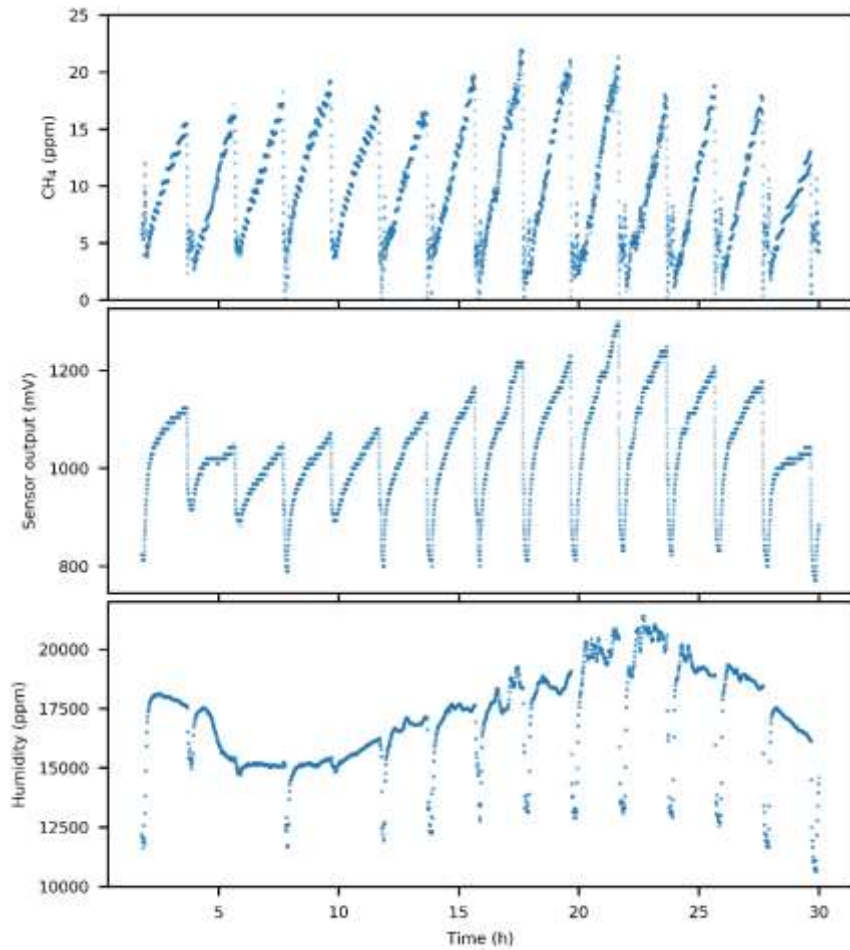
395 **Figure 3:** Real data from a flux chamber on a lake in June 2019 with 14 automated chamber open-closure cycles over 30 hours. The upper, central and bottom panels show calibrated CH_4 mole fractions based on this study, untreated sensor output signal, and absolute humidity.